

# $\text{Al}_{0.95}\text{Ga}_{0.05}\text{As}_{0.56}\text{Sb}_{0.44}$ for lateral oxide-confinement layer in InP-based devices

M. H. M. Reddy<sup>a)</sup>

*Department of Electrical and Computer Engineering, University of California, Santa Barbara, California 93106*

D. A. Buell, A. S. Huntington

*Department of Materials Science, University of California, Santa Barbara, California 93106*

T. Asano, R. Koda, D. Feezell, D. Lofgreen and L.A. Coldren

*Department of Electrical and Computer Engineering, University of California, Santa Barbara, California 93106*

## **Abstract**

We report a new lateral oxide confinement layer for InP-based devices using lattice matched AlGaAsSb. The confinement layer induced excess loss at different widths was extracted after de-embedding the losses due to carrier diffusion, non-radiative recombination and changes in internal injection efficiency. Results show that AlGaAsSb-oxide acts as an excellent confinement layer, showing no excess loss down to a width 4  $\mu\text{m}$ .

PACS: 81.05.Ea, 81.15.Hi, 42.55.Px

<sup>a)</sup>Electronic mail: mreddy@ece.ucsb.edu

The importance of current and optical confinement layers has been well demonstrated in the GaAs-based vertical-cavity surface emitting lasers in terms of attaining ultra-low thresholds and higher wall-plug efficiency.<sup>1</sup> Native AlAs-oxide was used as a confinement layer in these devices. Unfortunately extremely high lattice mismatch prevents using this oxide in long wavelength ( $>1.3\mu\text{m}$ ) devices grown on InP. Ironically, the need for a confinement layer is more pronounced in these devices due to enhanced Auger recombination, carrier spillage out of quantum wells due to small carrier confinement and larger thermal impedance. Predictably, many materials were explored for this purpose and Table I lists all the materials investigated to date. Also listed is the InP congruent evaporation temperature for comparison. It is clear from the Table that AlInAs is not useable due to high oxidation temperature ( $T_{ox}$ ) and low oxidation ( $R_{ox}$ ) rate. Alloys with larger Al concentration, using strained epitaxial layers and superlattices, were to some extent successful in enhancing the  $R_{ox}$  but not in lowering the  $T_{ox}$ . As we can see, amongst all materials listed in Table I, AlAsSb and AlGaAsSb with high Al content show the lowest  $T_{ox}$  and reasonable  $R_{ox}$ . The main problem with implementing above material as the confinement layer arises from the observation that when a bulk layer (about 100 nm thick or more) of AlAsSb oxidizes, it tends to segregate into Aluminum oxide and Sb metal and this Sb metal shows up as bright contrast layer in SEM picture as shown in Fig 1. Such metal segregation may be fatal to device performance due to increased optical loss and leakage current. We have recently reported that the  $R_{ox}$  of AlGaAsSb is more reproducible than the ternary, AlAsSb, and that edge emitting lasers enclosing AlGaAsSb-oxide show no noticeable current leakage, and

optical losses at confining layer widths ( $W$ ) as small as 6.5  $\mu\text{m}$ , possibly indicating no Sb segregation<sup>7</sup>.

In this letter, we report the AlGaAsSb-oxide induced excess loss as a function of  $W$  by extracting internal injection efficiency and internal loss at each  $W$  from a set of edge emitting lasers with different stripe lengths and comparing with those derived from broad-area lasers without oxidation.

Varian Gen II solid state MBE system was used to grow broad area edge emitting laser structures enclosing a 20nm thick AlGaAsSb as shown in Fig. 2(a). More details about growth procedure were mentioned elsewhere<sup>7</sup>. The energy band diagram, in Fig. 2(b), shows a large conduction-band discontinuity at AlGaAsSb/AlInAs interface, suggesting the added advantage of blocking the electrons that spill out of the active region at higher operating temperatures. It has been reported earlier that such electron blocking improves the characteristic temperature of long-wavelength lasers<sup>3</sup>. Also of importance is the valance-band discontinuity at the above interface. Unless otherwise p-doped, this discontinuity acts as a barrier for hole injection and also increases the diode turn-on voltage. Both these characteristics were observed in this case, as the AlGaAsSb is undoped. Mesas of different stripe widths were wet-etched using PECVD deposited oxide/nitride layers as a protective mask. Subsequently, these samples were subjected to wet-oxidation at 365°C for different lengths of time. For more details about oxidation, please refer to our previous paper<sup>7</sup>. Interestingly enough, the cross-sectional SEM in Fig. 2(c) does not show any bright Sb-metal contrast around the oxide interface. After

removing the oxide/nitride protective mask, Ti/Pt/Au metal was deposited as the p-contact layer. Samples were then thinned down to about 100  $\mu\text{m}$ , followed by the deposition of Ni/AuGe/Ni/Au as the n-contact layer. Finally, samples were subjected to post-metal anneal in forming gas at 380°C for a few seconds. Edge emitting lasers of different lengths were then cleaved and left un-coated while testing. A cleaved bar from each sample was used to determine the oxidation depth using cross-sectional SEM.

Initially,  $L$ - $I$ - $V$  curves under pulsed conditions were recorded for lasers enclosing AlGaAsSb layer with no oxidation to extract differential efficiency ( $\eta_d$ ) and threshold currents ( $I_{th}$ ). For this study, stripes of 20  $\mu\text{m}$  width and cavities longer than 500  $\mu\text{m}$  were used. From the linear curve-fit of  $1/\eta_d$  versus cavity length,  $L$ , the internal injection efficiency ( $\eta_i$ ) and modal internal loss ( $\langle\alpha_i\rangle$ ) were calculated as shown in the equation,

$$\frac{1}{\eta_d} = \frac{\langle\alpha_i\rangle}{\eta_i \ln(1/R)} L + \frac{1}{\eta_i}, \quad (1)$$

where  $R$  is the mean mirror intensity reflection coefficient (for InP based cleaved facet devices, it is generally taken as 0.32). Threshold modal gain was calculated for each  $L$  using,

$$\Gamma g_{th} = \langle\alpha_i\rangle + \frac{1}{L} \ln\left(\frac{1}{R}\right), \quad (2)$$

where  $\Gamma$  is the cavity confinement factor, which is derived for this structure as 4.5%. A plot was then constructed between  $\Gamma g_{th}$  versus threshold carrier density ( $N_{th}$ ), determined from  $I_{th}$  values using,

$$\frac{\eta_i I_{th}}{qV} = B N_{th}^2 + C N_{th}^3, \quad (3)$$

where the bimolecular recombination coefficient,  $B$  and the Auger recombination coefficient,  $C$  are taken as  $10^{-10}$  cm<sup>3</sup>/s and  $8 \times 10^{-29}$  cm<sup>6</sup>/s respectively and  $V$  is the gain region volume. By curve-fitting the data to,

$$g_{th} = g_o \ln\left(\frac{N_{th}}{N_{tr}}\right), \quad (4)$$

the gain coefficient  $g_o$  and transparency carrier density  $N_{tr}$  can be extracted as fitting parameters.

In a similar way, we have extracted  $I_{th}$ ,  $\langle\alpha_i\rangle$  and  $\eta_i$  values for lasers enclosing oxide confinement layers of varying  $W$ . Since carrier diffusion is a dominating loss mechanism at smaller  $W$ , the following carrier diffusion equation was solved numerically to obtain carrier profile along the x-direction.

$$D \frac{\partial^2 N(x)}{\partial x^2} = -\frac{\eta_i I_{th}(x)}{Aq} + \frac{N(x)}{\tau} \quad (5)$$

where,  $D$  is the ambipolar diffusion coefficient and  $\tau$  is the carrier lifetime that takes care of defect, spontaneous and Auger recombination put together. A wide range of data agreed to the values of 15 cm<sup>2</sup>/s and 1.7 ns for  $D$  and  $\tau$  respectively. Then the gain profile in the x-direction,  $g(x)$  was calculated by substituting  $N(x)$  for  $N_{th}$  in Eq. (4). Gain profile can then be weighted by normalized mode intensity along x-direction to obtain  $\Gamma_x g_x$ . The cavity modal gain,  $\Gamma g$  was then obtained by,

$$\Gamma g = \Gamma_x g_x \Gamma_{yz}, \quad (6)$$

where,  $\Gamma_{yz}$  is the confinement factor both in y and z-directions. Calculated gain from Eq. (6) and experimentally observed gain from Eq. (2) at each  $W$  were compared to find confinement layer induced excess loss.

Figure 3 shows L-I-V curves at different  $W$ . As can be seen from figure,  $I_{th}$  reduces monotonically with decreasing  $W$  down to 4  $\mu\text{m}$  and then increases abruptly at 3.5  $\mu\text{m}$ . From the slopes of  $L-I$  curves, it can be seen that the differential efficiency remained almost unchanged till 4  $\mu\text{m}$  and decreases at 3.5  $\mu\text{m}$ . From the  $I/\eta_d$  versus  $L$  curves in Fig. 4, it can be seen that both the intercepts and slopes, in other words, the  $\eta_i$  and  $\langle\alpha_i\rangle$  remain unchanged till 4  $\mu\text{m}$  and are adversely affected at 3.5  $\mu\text{m}$ . Experimentally measured excess internal loss, which is the difference between  $\langle\alpha_i\rangle$  of oxide-confined and broad-area lasers respectively, shows no oxide-induced excess loss till 4  $\mu\text{m}$  and increases to about 0.3% per pass at 3.5  $\mu\text{m}$  (Fig.5). On the other hand, the  $J_{th}$  versus  $W$  curve, shown in Fig. 5, indicates a mild increase in  $J_{th}$  as  $W$  reduces from 7  $\mu\text{m}$  to 4  $\mu\text{m}$  and then an abrupt increase at 3.5  $\mu\text{m}$ . Also drawn in Fig. 6 is excess current loss, which is the difference between the measured terminal  $I_{th}$  and the current calculated from gain curve to match the experimentally observed threshold modal gain. Excess current remains almost zero till 4  $\mu\text{m}$  and then rises to about 40% at 3.5  $\mu\text{m}$ .

The fact that the  $\eta_d$  remains unaffected even as  $W$  reduces to 4  $\mu\text{m}$  and the mode penetrates it more indicates that the Sb segregation problem might have been totally eliminated in this case. We believe that, for thin layers at such low oxidation rates, homogeneous oxidation of Al, Sb and As may take place together and the oxides of As

and, to some extent Sb, being volatile may leave the layer and the remaining Sb-oxide may form a homogeneous phase with  $\text{Al}_2\text{O}_3$ . SEM picture, in Fig. 1 (c), confirms this by not showing any bright Sb metal contrast.

Diffusion of carriers beneath the oxide-confinement layer plays an important role at smaller  $W$ , solely accounting for the rise in  $J_{th}$  till  $4 \mu\text{m}$  and about 25% at  $3.5 \mu\text{m}$ . Several reasons may be attributed to the 40% excess  $J_{th}$  loss recorded at  $3.5 \mu\text{m}$ . It is unlikely that leakage current might have played a role here as the pre-turn on characteristics of I-V curves in Fig. 3 indicated no sign of it. Carrier lifetime,  $\tau$ , assumed in this case as constant, is generally a function of  $N$ .  $\tau$  reduces with increasing  $N$ , as is generally the case at smaller  $W$ , which in turn increases the carrier loss. Other factors that might have contributed to the excess carrier loss included the deterioration of uncoated mirror facets at smaller widths and surface recombination at oxide/semiconductor interface.

In conclusion, we have demonstrated lossless AlGaAsSb-oxide confined edge emitting lasers down to a layer width of  $4 \mu\text{m}$ . At  $3.5 \mu\text{m}$ , lateral carrier diffusion contributes more to the increase in  $J_{th}$  than the internal optical loss. Results suggest that thin AlGaAsSb layer at low oxidation temperatures oxidizes homogeneously leaving no Sb metal segregation behind.

## References

1. E. R. Hegblom, N.M. Margalit, A. Fiore, and L.A. Coldren, IEEE J. Sel. Top. Quant. Electron., **5**, 553 (1999).
2. H. Geebretsadik, K. Kamath, W-D. Zhou, P. Bhattachrya, C. Caneau, and R. Bhat, Appl. Phys. Lett. **72**, 135 (1998).
3. N. Ohnoki, F. Koyama, and K. Iga, J. Crystal Growth, **195**, 603 (1998).
4. E. Hall, A. Huntington, R. L. Naone, H. Kroemer, and L. A. Coldren, J. Electr. Mater., **29** 1100 (2000).
5. M. Linnik, and A. Christou, IEEE Trans. Electron Devices, 48, 2228 (2001).
6. J.-H. Shin, B. -S. Yoo, W.-S.Han, O. -K. Kwon, Y. -G. Ju, and J. -H. Lee, IEEE Photon. Technol. Lett., **12**, 1031 (2002).
7. M. H. M. Reddy, D. A. Buell, T. Asano, R. Koda, D. Feezel, A. S. Huntington, and L. A. Coldren, Submitted to J. Crystal Growth.

Table I. List of materials used for lateral oxide-confinement layer in InP-based devices.

Material	$T_{ox}$ (°C)	$R_{ox}$ ( $\mu\text{m/hr}$ )	Comments	Ref.
AlInAs	475	0.5	High $T_{ox}$ , slow rate	2
AlAs/AlInAs Superlattices	470	5	High $T_{ox}$ , large strain	3
AlAs/InAs Superlattices	525	6.0	High $T_{ox}$ , large strain	4
AlInAsP	375	0.06	Slow $R_{ox}$	5
$\text{Al}_{0.6}\text{In}_{0.4}\text{As}$	485	2.0	High $T_{ox}$ , strain	6
AlAsSb/ AlGaAsSb	350/ 365	5.75 3.6	Low $T_{ox}$ , reasonable $R_{ox}$	7

## List of Figures

Fig.1. A schematic showing segregation of thick AlAsSb layer into  $\text{Al}_2\text{O}_3$  and Sb metal during oxidation. SEM picture shows bright contrast due to Sb metal at the interface.

Fig. 2. Edge emitting laser enclosing AlGaAsSb-oxide confinement layer. (a) Layer structure, (b) Energy-band diagram and (c) Cross-sectional SEM picture showing the oxide-confinement layer.

Fig. 3.  $L$ - $I$ - $V$  curves of edge emitting lasers enclosing AlGaAsSb-oxide confinement layer of different widths ( $W$ ).

Fig. 4. Inverse differential efficiency versus cavity length for different confinement widths ( $W$ ).

Fig.5. Difference between the  $\langle\alpha_i\rangle$  of oxide-confined and broad-area lasers drawn as excess modal loss versus confinement layer width ( $W$ ).

Fig. 6.  $J_{th}$  versus confinement layer width. Excess current loss is the difference between measured  $I_{th}$  and the calculated current from gain curve for the same threshold modal gain.

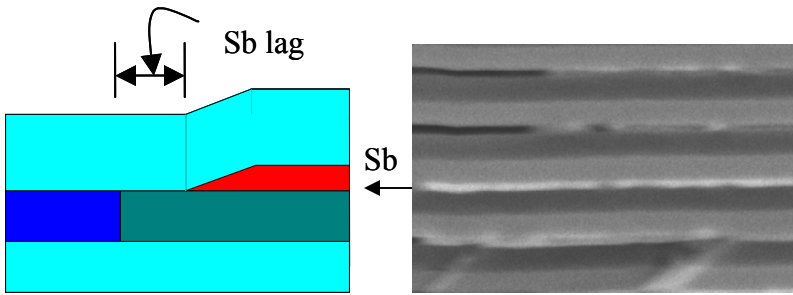


Figure 1  
M. H. M. Reddy et al.

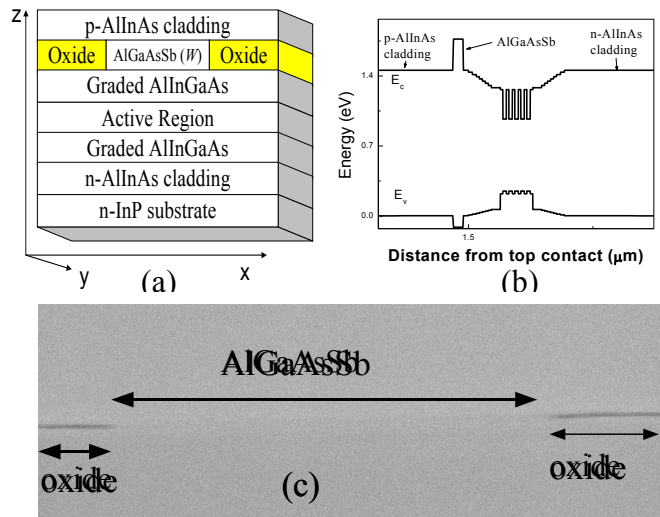


Figure 2  
M. H. M. Reddy et al.

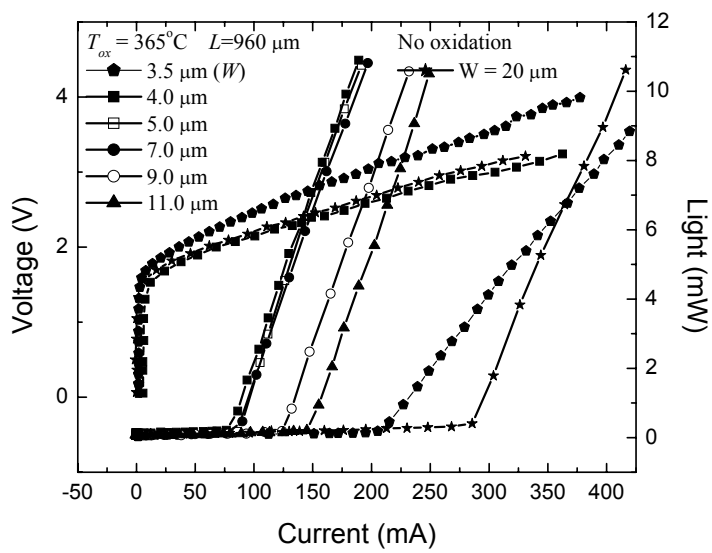


Figure 3  
M. H. M. Reddy et al.

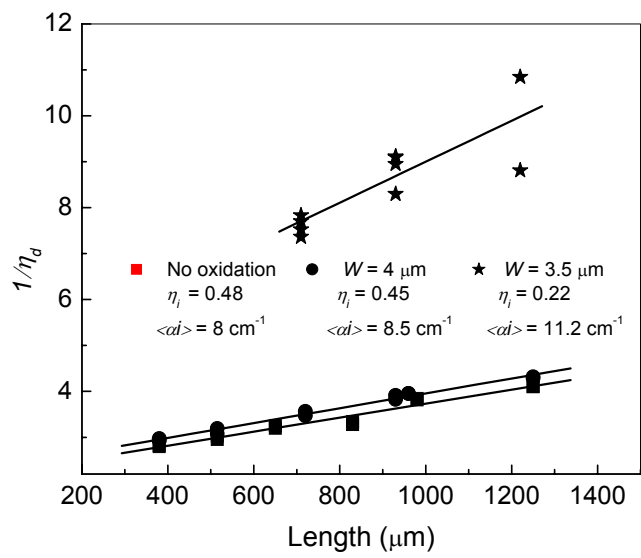


Figure 4  
M. H. M. Reddy et al.

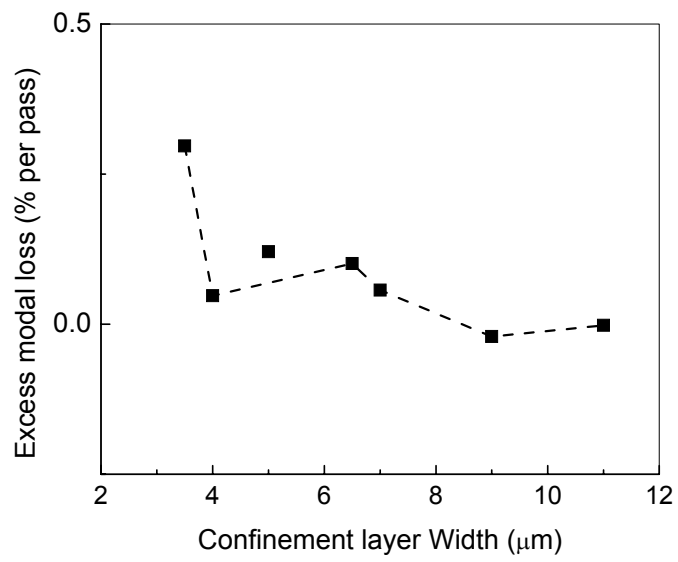


Figure 5  
M. H. M. Reddy et al.

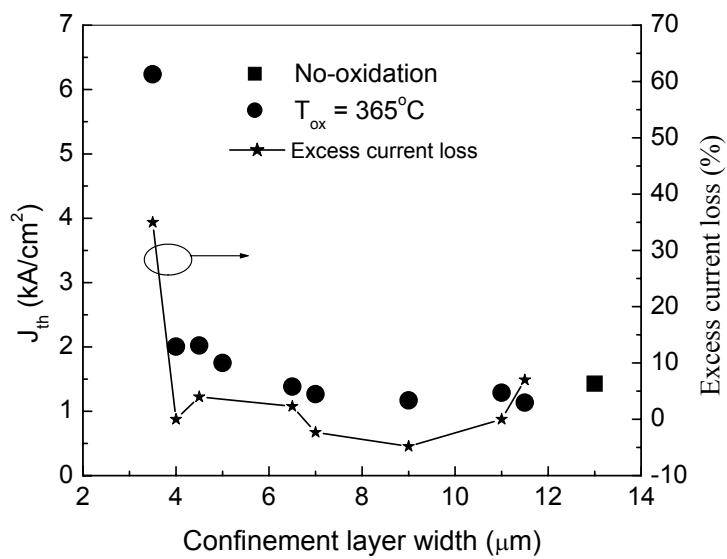


Figure 6  
M. H. M. Reddy et al.